Proceedings of ASME Turbo Expo 2011
GT2011
June 6-10, 2011, Vancouver, British Columbia, Canada

GT2011-46804

EFFECT OF SURFACE TEXTURING ON THE STEADY-STATE PROPERTIES AND DYNAMIC COEFFICIENTS OF A PLAIN JOURNAL BEARING: EXPERIMENTAL STUDY

Azzedine Dadouche*, Martin J. Conlon and Waldemar Dmochowski
Gas Turbine Laboratory
Institute for Aerospace Research
National Research Council
Ottawa, Ontario, Canada

Waldemar Koszela, Lidia Galda and Pawel Pawlus
Rzeszow University of Technology
Department of Manufacturing Processes and Production Organization
35-959 Rzeszow, Poland

ABSTRACT

The last decade has seen a significant and increased interest in surface texturing technologies esulting in improving the overall tribological properties of mechanical components. Several techniques could be used to modify the surface topography with laser surface texturing becoming most popular recently.

In this investigation, rig experiments have been performed on plain and textured-surface journal bearings with an aspect ratio of 1.1 under a variety of loads and speeds. Percussive burnishing (embossing) was used to create the dimples on the internal surfaces of the test bearings. The dimples have a spherical shape with a diameter of 1 mm and a depth of 60 micrometers. Pit-area ratio was in the range 5-20% of the total bearings surfaces. The effects of surface-texturing and dimple density on the bearing steady-state characteristics and dynamic coefficients are analyzed and discussed in this paper.

NOMENCLATURE

BB:	Baseline bearing
TXT1:	Lightly textured bearing
TXT2:	Medium textured bearing
TXT3:	Highly textured bearing
TXT4:	Intensely textured bearing
m_b:	Bearing assembly mass
x'', y'':	Bearing acceleration in horizontal and vertical directions (time domain)
x', y':	Bearing velocity in horizontal and vertical directions (time domain)
x, y:	Bearing displacement in horizontal and vertical directions (time domain)
f_x, f_y:	Excitation force in the horizontal and vertical directions (time domain)
b_{ij}	Direct and cross –coupling damping coefficients
k_{ij}	Direct and cross –coupling stiffness coefficients
ω:	Frequency
F_x, F_y:	Excitation force in the horizontal and vertical directions (frequency domain)
A_x, A_y:	Bearing acceleration in horizontal and vertical directions (frequency domain)
X, Y:	Bearing displacement in horizontal and vertical directions (frequency domain)
H_{ij}:	Direct and cross-coupling frequency response function

INTRODUCTION

Recently, surface texturing has attracted the attention of tribologists since it can be used to improve tribological properties of sliding elements without changing either the materials or the lubricants. Surface texturing is a surface engineering technique that results in improved tribological properties such as coefficient of friction, wear resistance, etc. The oil pockets (dimples) may reduce friction and act as micro-hydrodynamic bearings in cases of full or mixed lubrication, and/or by acting as lubricant reservoirs in cases of starved lubrication. The dimples can also be micro-traps to capture pollution and wear debris in lubricated or dry sliding [1, 2]. Such depressions should be large enough to trap and store the particles. Experimental works investigating various forms and shapes of oil pockets have been carried out worldwide [3-6]. Various techniques can be employed for surface texturing such as: laser texturing, ion beam texturing, etching techniques and machining. The most familiar practical example of surface texturing is plateau honing of cylinder liner surfaces. Surface texturing is applied in bearings (journal bearings, thrust bearings and air bearing sliders). The friction characteristic of a journal bearing with dimple bushing manufactured using machining and chemical etching was investigated by Lu and Khonsari [7]. It was shown that with proper dimple dimensions the friction performance of journal bearings can be improved, particularly for light oils. Etsion et al. [8] studied the scuffing

* *Corresponding author*

resistance of piston pin bearings. Tests were performed on a baseline standard piston pin material, a laser surface textured (LST) pin, and coated pins with chromium nitride (CrN) and diamond-like carbon (DLC). The dimples occupied about 10% of the LST pin area and had a spherical shape with a diameter of 100 µm and a depth of 3 µm. Overall, the surface engineered pins performed better than the standard material. The LST pin provided the best bearing performance in terms of friction coefficient, scuffing inception and running temperature. It has also been shown that partial LST substantially improved load carrying capacity of parallel hydrodynamic thrust bearings [9]. The same technique seemed to reduce the friction coefficient by up to 25% in piston rings as stated by Ryk and Etsion [10].

Zhang and Qiu [11] numerically analyzed the effects of surface roughness (longitudinal, transverse and isotropic) on the performance of dynamically loaded journal bearings. The authors showed that all roughness types affect the minimum film thickness and maximum pressure (increase or decrease) depending on the bearing dimensions, clearance and mass. The isotropic roughness, which could be considered as dimples across the bearing surface, resulted in a thinner film thickness for all studied cases. Yong and Balendra [12] performed CFD simulations where they discussed the effect of surface texturing using LST on the performance of hydrodynamic contacts. The model did not take into account thermal effects nor body forces and was limited to studying two parallel plates with a single dimple on the moving part. The authors noted that LST led to a reduction in both friction and load carrying capacity. Increasing the depth of the dimples lowered the friction coefficient. The latter effect was also recently observed by Bouyer and Fillon [13] in their experimental investigation of friction coefficient measurements of journal bearings at start-up where they showed that, for bronze bushes, increasing the height of the isotropic roughness leads to a lowered startup friction coefficient.

Cupillard et al. [14] reported in their CFD analysis of journal bearings that friction coefficient could be significantly reduced if the dimples were located in the maximum pressure region or downstream the maximum film depending on the eccentricity ratio and dimple depth. It has also been shown that surface texturing leads to increased bearing load capacity at low eccentricity (lower that 0.25); however, higher eccentricities have a reverse effect.

Dimple shape and geometrical parameters and their effect on the frictional properties of materials in sliding contact have been investigated by a number of authors [15-17]. Wakuda et al. [15] studied the effect of surface micro-dimpling on the frictional properties of ceramic and steel under lubricated sliding contact using pin-on-disk tester at a very high contact pressure (0.78 GPa). The authors concluded that a dimple diameter around 100 µm with a density ranging between 5 to 20% produced a significant reduction in friction. They also noted that dimple profile had only limited effect. In a similar way, Galda et al. [17] have shown that a dimple density below 20% is very beneficial during the transition from mixed to hydrodynamic lubrication.

In this paper, an experimental analysis was carried out to study the effect of spherical-shaped dimples on the steady-state and dynamic properties of plain journal bearings. Four textured bearings with different dimple densities were tested in addition to a smooth surface bearing. It has been demonstrated that the dimples lead to a decrease in load carrying capacity and a significant increase of bearing stiffness.

TEST BEARINGS & TEXTURING TECHNIQUE

A number of plain journal bearings have been made from a Tin Bronze Alloy (CuSn10P) having a hardness of 138 HB. They feature an inner diameter of 36.04 mm (1.419 in) and a length of 39.62 mm (1.56 in). Their inner surfaces have been textured but one kept as a baseline bearing (BB). Percussive burnishing technique with electromagnetic drive [18] was used to create spherical oil pockets (dimples). During the burnishing process, the frequency and rotational speed were kept constant at 450 strokes per minute and 35.5 rpm respectively. The feed represents an input parameter and was equal to: 0.5 mm/rev. (19.69 mil/rev.), 0.75 mm/rev. (29.53 mil/rev.), 1.5 mm/rev. (59.06 mil/rev.) and 2.5 mm/rev. (98.43 mil/rev.). The area occupied by the oil pockets was in the range of 5-20% of the total bearing inner surface. Four distinct dimple-densities have been created on the bearings which could be identified as lightly-textured bearing (TXT1), medium-textured bearing (TXT2), highly-textured (TXT3), and intensely textured bearing (TXT4) as shown in Figure 1. The depth and diameter of the dimples was about 60 µm (2.36 mil) and 1 mm (39.37 mil) on average respectively. All textured specimens were turned using a CNC machine prior to burnishing resulting in an average roughness Ra of 0.76 µm (0.03 mil).

It is important to point out that the dimples had smooth edges because their depths were comparatively small (about 60 µm) for rather big diameters (about 1 mm) and the height of surface topography after a precise turning (before percussive burnishing) was quite high (6-8 µm). Therefore no material pile-up was observed on the surface topography profiles along the edges of the dimples.

Figure 2 shows a schematic of the burnishing machine used to plastically modify the surface topography of the test bearings. The machine has a frequency range of 2-15 kHz and is capable of burnishing 85 mm (3.35 in) long cylinders. It uses an impulse method (making use of kinetic energy of the working elements) to create the dimples using the burnishing tool which acts as a hammer on the bearing surface. During voltage feeding of the driving coil, a magnetic field affects the ferromagnetic core and pulls it inside the coil. The core is connected by a flexible connector with the arm. The oil pockets are formed as the result of short-time percussive impulses. The arrangement of oil pockets depends on rotational and feed speeds as well as stroke frequency, but shape depends on the burnishing element shape.

TEST RIG & INSTRUMENTATION

This experimental study was performed using a journal bearing test rig (Figure 3) which allows the measurements of bearing steady-state and dynamic properties. The rig is composed of a simply-supported shaft on two pairs of angular contact rolling bearings with the test section located at its mid-span. The shaft is driven by a 37 kW (50 hp) electric motor using a pulley-belt arrangement and rotates at speeds up to 16,500 rpm. Radial static loads of up to 22.25 kN (5,000 lb) can be applied to the test bearing using a hydraulic cylinder (located on top of the test bearing). The rig is also capable of applying single- and multi-frequency computer-controlled dynamic loads via two orthogonal electromagnetic shakers attached to the test bearing housing through a stinger-flexure mechanism. Each shaker is capable of applying a dynamic load of up to 1,335 N (300 lb). More details on the rig's test capabilities are presented in Table 1. A three-piece shaft design (instead of a single integral shaft) was used to reduce bearing assembly/disassembly period. The three parts have locking tapers at their ends (males and females) and were held together using a drawbar mechanism.

Two orthogonal single-axis accelerometers were installed on the bearing housing to measure steady state and dynamic bearing vibration response. The bearing location/orbit was monitored using eight proximity probes attached in orthogonal pairs at each side of the test bearing (two pairs per side). The accuracies of the accelerometers and proximity probes are ±0.098 m/s^2 (±0.01 g) and ±2.5 μm (±0.0001 in) respectively. Lubricant flow rate, supply pressure, oil bearing inlet and outlet temperatures as well as support bearing temperatures are monitored and measured during the tests.

The five test journal bearings (one baseline and four textured) were instrumented with seven type-T thermocouples (TC1-TC7) located circumferentially at the bearing mid-section 1 mm (39.37 mil) away from the running surface as shown in Fig. 4. Table 2 gives the angular location of each thermocouple. All bearings have the same aspect ratio of 1.1 and a nominal radial clearance ranging from 48.5 to 52.5 μm (1.91 to 2.07 mil) as presented in Table 3.

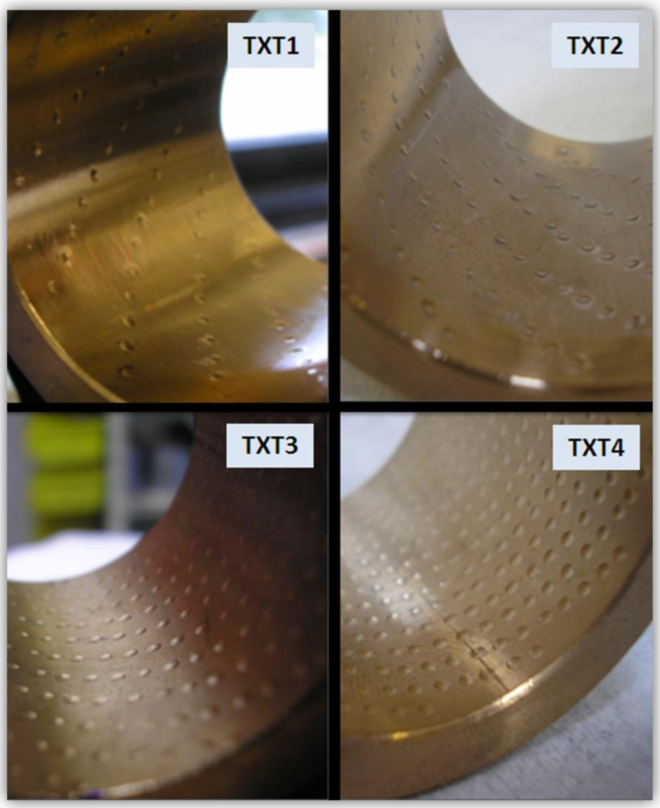

FIGURE 1. DIMPLES DISTRIBUTION ON TEST BEARINGS

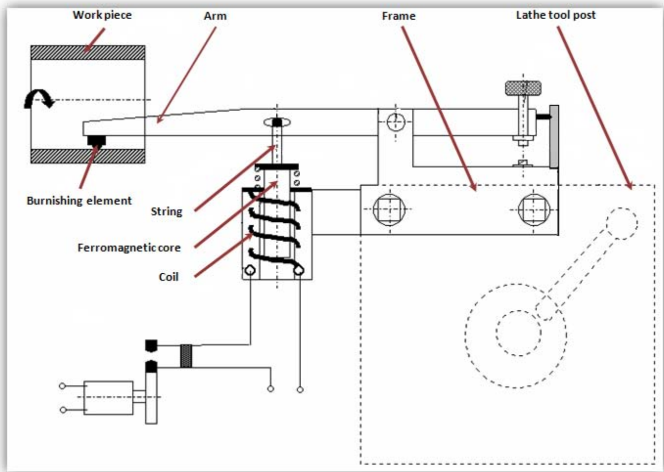

FIGURE 2. SCHEMATIC OF THE BURNISHING MACHINE

The bearings have been tested under a variety of speeds and radial loads for both steady-state and dynamic testing configurations. Table 4 shows the conditions at which the experiments have been performed. The note NAB (Not All Bearings) in this table implies that this specific test condition could not be achieved for at least one bearing as will be discussed in the next section. The value (amplitude) of the dynamic load (not shown in Table 4) may not be constant as it depends on the bearing operating conditions and is limited by either the total allowable bearing displacement or force transducer/shaker capacity.

All bearings were lubricated using ISO-VG32 oil grade. The lubricant was fed to the bearing from top through a radial hole at a constant temperature of 49 °C (120 °F).

The data were acquired using a high-speed, portable, 24 bit data acquisition system with a bandwidth capability of 25.6 kHz. All signals were acquired at a sampling rate of 10,240 Hz.

TABLE 1. DYNAMIC RIG OPERATION CAPABILITIES

Parameter	Capability (up to)
Journal diameter	100 mm (~4 in)
Shaft speed	16,500 rpm
Static load	22250 N (~5,000 lb)
Dynamic load	1335 N (~300 lb)
Frequency of excitation	20 to 7500 Hz
Lubricant flow rate	38 L/min (~10 USgpm)
Lubricant supply temperature	95 °C (~200 °F)
Power	37 kW (50 hp)

TABLE 2. THERMOCOUPLE ANGULAR LOCATION

Thermocouple	TC 1	TC 2	TC 3	TC 4	TC 5	TC 6	TC 7
Location (°)	30	135	180	195	210	240	300

TABLE 3. TEST BEARING CLEARANCE

Test bearing	Nominal clearance
Smooth (BB)	51.5 µm (2.03 mil)
Light textured (TXT1)	52.5 µm (2.07 mil)
Medium textured (TXT2)	52.0 µm (2.05 mil)
High textured (TXT3)	50.0 µm (1.97 mil)
Intense textured (TXT4)	48.5 µm (1.91 mil)

TABLE 4. TEST CONDITIONS

Parameter		Speed (rpm)			
		2,000	5,000	8,000	10,000
Static load	2225 N (500 lb)	✓	✓	✓	✓
	4000 N (900 lb)	NAB	✓	✓	✓
	5340 N (1200lb)	NAB	✓	✓	✓

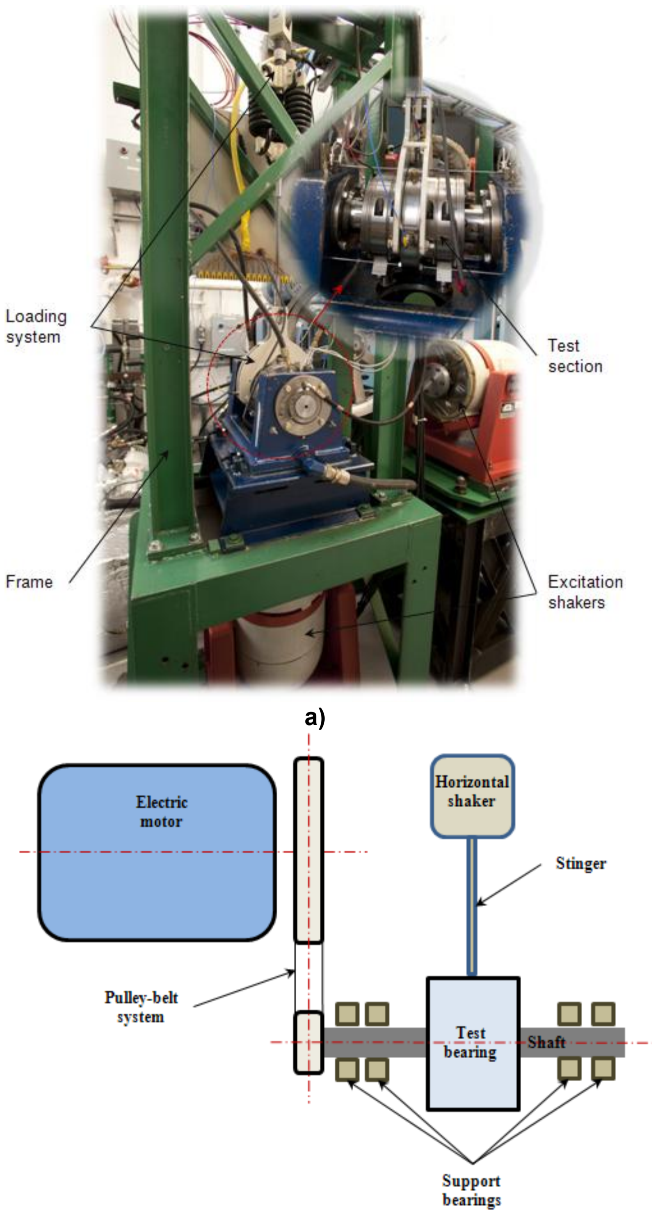

FIGURE 3. DYNAMIC JOURNAL BEARING TEST RIG: a) general view, b) schematic of the rig

EXPERIMENTAL PROCEDURE

Test procedures have been defined and set depending on the test requirements. For steady-state experiments, the instructions are as follows:

1. Run the data acquisition system
2. Set the correct oil flow rate and adjust oil supply temperature
3. Lift the bearing to its neutral position
4. Acquire neutral position signals
5. Start the motor and slowly ramp up the speed until the lowest test speed is reached.
6. Slowly apply the desired radial load to the test bearing using the hydraulic loading system.
7. Adjust the bearing oil inlet temperature at 49 °C (±1 °C).
8. Wait at least 5 min to allow for thermal balance and bearing temperatures to stabilize.
9. Record data.
10. Repeat sequences 6 to 9 for the next loads.
11. Reduce load to the lowest required value, increment speed to the next test condition and repeat sequences 7 to 11.

The dynamic testing requires the connection of the stingers prior to starting the rig. Only one stinger (horizontal or vertical) is attached at a time. The same steady-state test sequences apply to dynamic testing with the exception of dynamically exciting the bearing with an engineered multi-frequency signal prior to recording the data. The bearing dynamic movement (peak value) was kept below 15% of the bearing clearance. The periodic waveform used in this study is composed of 50 distinct frequencies, equally spaced between 20 and 250 Hz. The waveform individual frequencies were phase-shifted to minimize the overall peak-to-peak amplitude of the waveform and therefore each frequency of interest has the same power [19].

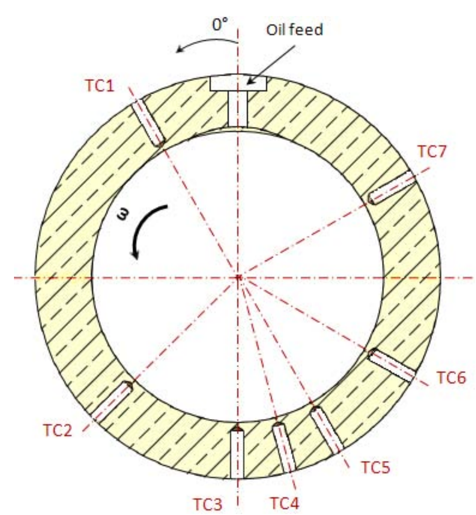

FIGURE 4. THERMOCOUPLE LOCATIONS ON TEST BEARINGS

RESULTS & DISCUSSION

Steady-State Characteristics

Figures 5 through 9 depict the dimensionless bearing center positions relative to the shaft centerline at various operating conditions. It is important to mention that these positions do not necessarily represent the bearing relative eccentricity as bearing-neutral positions were not accurately defined prior to steady-state testing. Offset factors have to be back-calculated and determined for each bearing in order to precisely calculate the actual bearing position and consequently the minimum film thickness. However, all figures show interesting trends under the effects of speed and static load. At the lowest load and for all bearing-types, the speed increase could result in instability situations as the bearing center gets closer to that of the shaft. The baseline plain bearing (Fig. 5) represents an unstable case with a high level of synchronous vibration for all test conditions especially at higher speeds. The bearing orbits around its static position and draws a donut which extends as the speed increases. The light textured bearing (Fig. 6) makes a significant difference with a dense orbit and firm location at all test conditions. TXT2 (Fig. 7) also shows very interesting results except for the lowest load and highest speed where its orbit slightly extends but not as significantly as BB. Textured bearing 3 (Fig. 8) shows strange trends which are mainly due to a rub that occurred at 2,000 rpm and 5,340 N. As the figure shows, the bearing performed well at 2,000 rpm and 2,225 and 4,000 N, respectively. When the rub occurred (at 5340 N) the bearing became unstable and responded randomly. Even though the bearing suffered severe wear with very high temperatures (Figs. 10-11), it did not fail and kept running smoothly after the incident. It is normal to see the bearing shifting position at higher speeds (Fig. 8) since the rub completely eliminated the dimples in the loaded area and consequently the clearance has significantly changed.

Further increasing the density of the dimples (TXT4) had a negative effect on the bearing behavior as shown in Fig. 9 where the bearing orbits are in the range of those of the baseline bearing or even a bit worse at some test conditions. In addition, the bearing load capacity was also reduced since tests at 2,000 rpm and loads higher than 3,500 N (~790 lb) could not be completed. Bearing temperature rose suddenly while increasing the load from 2,225 N to 4,000 N. The loading system was then deactivated to avoid severe wear or bearing failure. A very light and localized rub mark was noticed on the bearing surface during post-test inspection.

The tests of surface-textured bearings TXT3 and TXT4 suggest that increasing the dimple density weakens the oil film and affects its carrying action. Bearing clearance of both bearings are a bit low (Table 3) compared to the other bearings which could have had an additional effect on reducing their load capacity. This is in agreement with the literature as has been reported in [11, 12 and 14].

In the next section, the data obtained with the highly-textured bearing (TXT3) will not be presented due to its wear and clearance change. Also, the data obtained on TXT4 at 2000 rpm will be omitted.

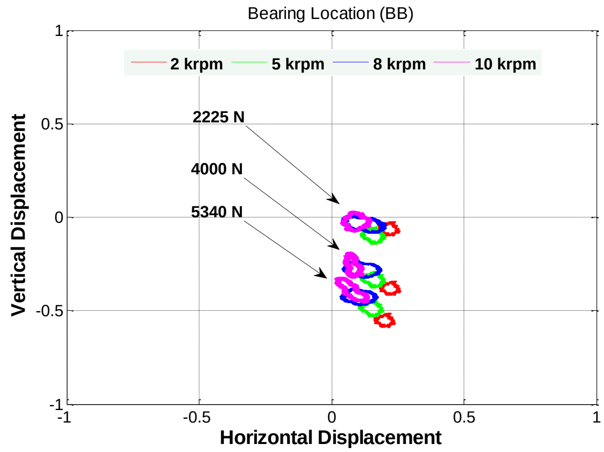

FIGURE 5. DIMENSIONLESS LOCATION OF BB

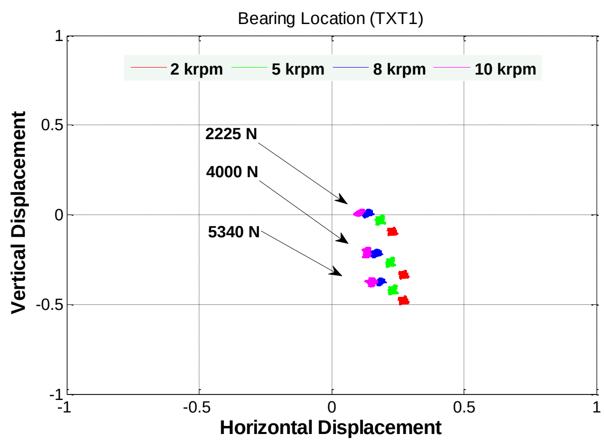

FIGURE 6. DIMENSIONLESS LOCATION OF THE TXT1

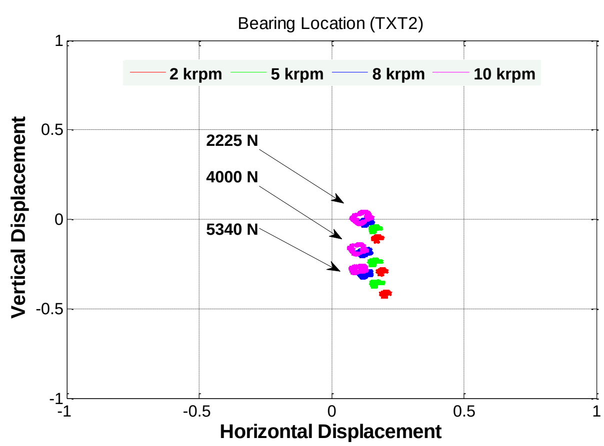

FIGURE 7. DIMENSIONLESS LOCATION OF THE TXT2

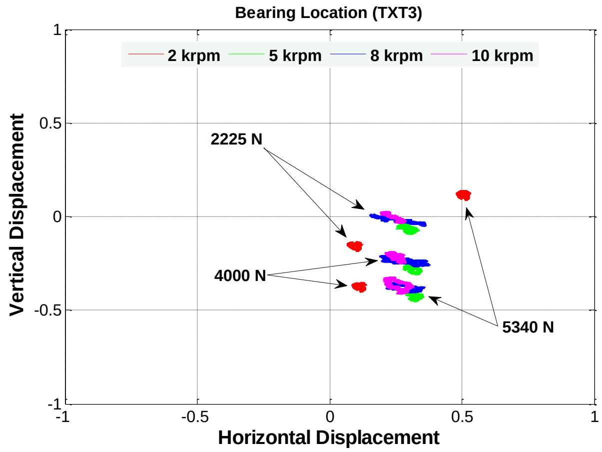

FIGURE 8. DIMENSIONLESS LOCATION OF TXT3

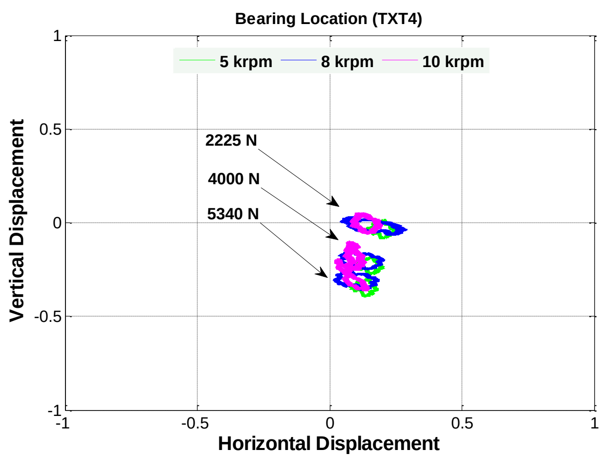

FIGURE 9. DIMENSIONLESS LOCATION OF THE TXT4

FIGURE 10. BEARING WEAR (TXT3)

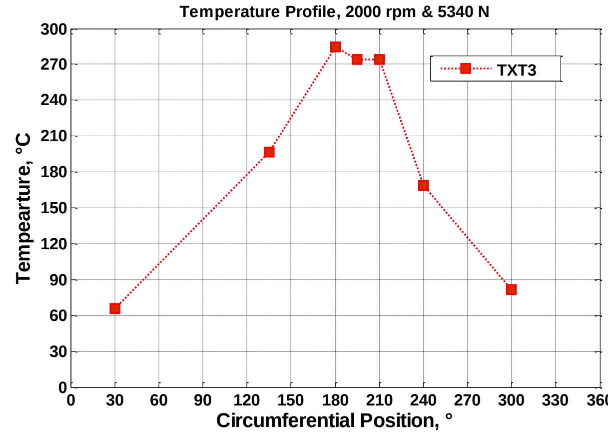

FIGURE 11. TEMPERATURE PROFILE OF THE WORN BEARING (TXT3)

The plain bearing angular temperature profile at the highest applied radial load (5,340 N) and various shaft speeds is presented in Figure 12. As one would expect, the figure depicts a typical bearing temperature profile where the hottest area is localized in the loaded section of the bearing (TC4 to TC6) where the thin film is highly stressed. The bearing cools down right after the diverging region. The figure also shows the effect of fresh oil on temperature (TC1) since the bearing was fed from its top dead center.

The combined effect of load and speed on the bearing (BB) maximum temperature (TC6) is presented in Figure 13. The load has a negligible effect on the bearing maximum temperature especially at low speeds. The increase rate is about 5% at low speeds and reaches 10% at a speed of 10,000 rpm. On the other hand, the shaft speed has a major influence on the temperature as the fluid shear-stress is proportional to speed. For example, the rise of the bearing maximum temperature (when the speed changes from 2,000 to 10,000 rpm) ranges from 41% to 46% for the three radial loads.

The combination of high load and speed produces the hottest point of the oil film.

In Figure 14, the effect of surface texturing on the bearing maximum temperature is depicted at the various test speeds and loads. As the figure shows, the temperature evolves similarly for all bearings with textured bearings running hotter than the baseline. A better picture of the temperature circumferential profile is presented in Figure 15. The plots confirm what has been mentioned in the previous section that the oil pockets tend to weaken the oil film and reduce its thickness especially in the loaded area. This affects the temperature values throughout the bearing section. The temperature increase ranges between 4% and 12.5% for all thermocouples with the maximum increase at TC2.

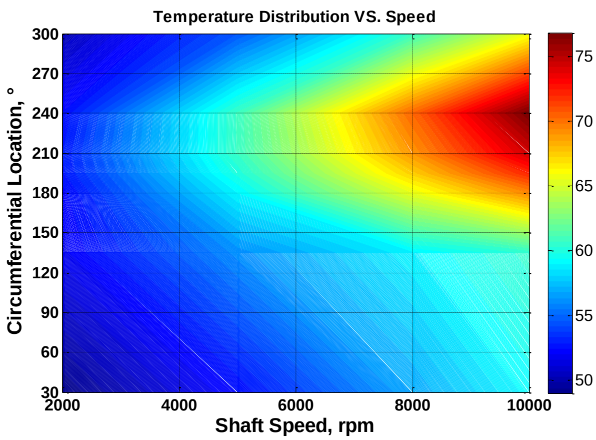

FIGURE 12. CIRCUMFERENTIAL DISTRIBUTION OF BEARING TEMPERATURE AT A CONSTANT LOAD OF 5340 N AND VARIABLE SPEEDS, BB

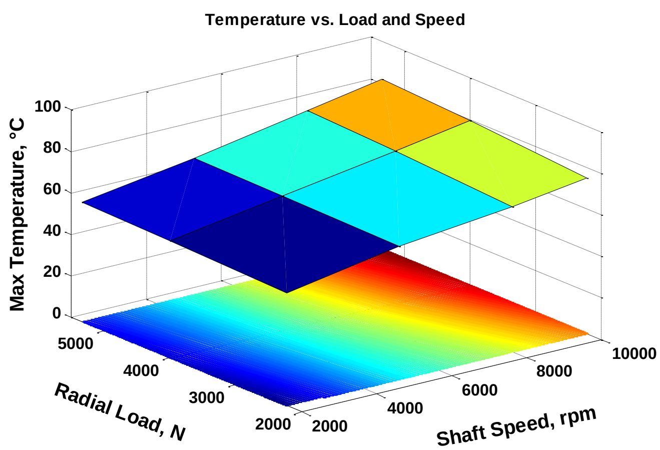

FIGURE 13. BEARING MAXIMUM TEMPERATURE (TC6) VERSUS SPEED AND LOAD, BB

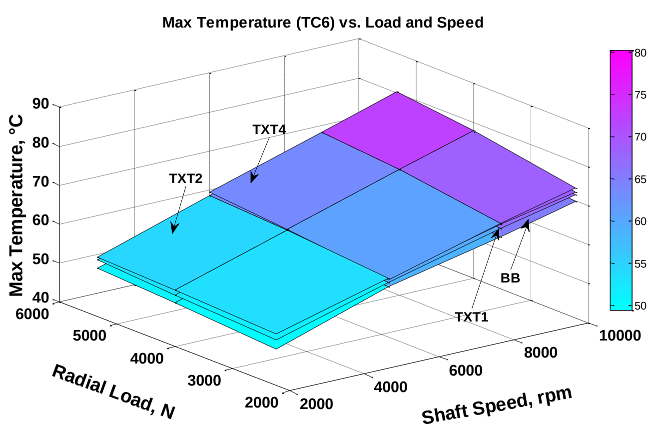

FIGURE 14. MAXIMUM TEMPERATURE VERSUS LOAD AND SPEED FOR BB, TXT1, TXT2 AND TXT4

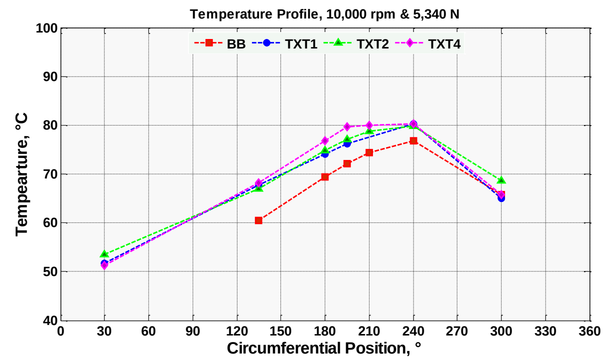

FIGURE 15. CIRCUMFERENTIAL TEMPERATURE PROFILE AT THE HIGHEST SPEED AND LOAD FOR BB, TXT1, TXT2 AND TXT4

Dynamic Coefficients

The determination of the bearing stiffness and damping coefficients is based on the Power Spectral Density method proposed by Rouvas and Childs [20] where a detailed description of the method is given.

In few words, this technique solves the bearing's equation of motion in the frequency domain and then evaluates its dynamic coefficients from the frequency response function (FRF). Equations (1) and (2) describe the bearing motion within its linear range in both time and frequency domains respectively.

$$m_b \begin{bmatrix} x'' \\ y'' \end{bmatrix} + \begin{bmatrix} b_{xx} & b_{xy} \\ b_{yx} & b_{yy} \end{bmatrix} \begin{bmatrix} x' \\ y' \end{bmatrix} + \begin{bmatrix} k_{xx} & k_{xy} \\ k_{yx} & k_{yy} \end{bmatrix} \begin{bmatrix} x \\ y \end{bmatrix} = \begin{bmatrix} f_x \\ f_y \end{bmatrix} \quad (1)$$

$$\begin{bmatrix} F_x(w) \\ F_y(w) \end{bmatrix} - m_b \begin{bmatrix} A_x(w) \\ A_y(w) \end{bmatrix} = \begin{bmatrix} H_{xx} & H_{xy} \\ H_{yx} & H_{yy} \end{bmatrix} \begin{bmatrix} X(w) \\ Y(w) \end{bmatrix} \quad (2)$$

In these equations, the excitation force is considered as the input to the system and the displacement and acceleration as outputs. Four equations are required to solve for the complex matrices H_{ij} from which stiffness and damping can be extracted ($H_{ij}=k_{ij}+i\,\omega b_{ij}$). The first two equations are obtained by exciting the bearing system in one direction and measuring displacement and acceleration in both directions and the second set of equations is obtained by exciting the system in the other direction and taking the same measurements.

Before starting the discussion of the bearings' dynamic properties, it is important to mention that Power Spectral Densities of the dynamic force, vibration and displacement showed the presence of a number of resonant frequencies. The main frequencies are located at 90 Hz, 125 Hz, 190 Hz and 275 Hz in the vertical direction and 65 Hz, 155 Hz, 175 and 200 Hz in the horizontal direction. Those beyond 150 Hz were strong spikes and significantly affected the nearby frequencies' amplitudes. Having said that, only the 20-150 Hz frequency range will be considered for the dynamic coefficient calculations.

Figure 16 illustrates the direct stiffness coefficients K_{xx} and K_{yy} of the baseline bearing at a constant rotational speed of 5,000 rpm and the various static test loads. Both coefficients feature a slight linear evolution as the frequency increases regardless of the static load. The latter has a significant effect on the coefficients especially K_{yy} where the stiffness increase represents about 57% when the load changes from 2,225 N to 5,340N. One would foresee this behavior as the oil film becomes thinner as the applied load gets higher.

Increasing the speed to 10,000 rpm (Fig. 17) had very little effect on the stiffness (as compared to Fig. 16) especially at the highest load where the bearing barely moves when the speed changes.

The bearing direct damping coefficients at a constant speed of 5,000 rpm and various loads may be visualized in Fig. 18. Except for the few spikes featuring some resonant frequencies in the bearing assembly system, both coefficients are more or less constant over the frequency range. Increasing the load tends to reduce the vertical damping which could be expected since the film gets stiffer. Stiffening the film shifts the bearing resonant frequency to higher values as one can notice the spike at 90 Hz moving to 95 Hz and then 100 Hz as the load increases. It is also worth mentioning that the vertical damping is about twice the horizontal at least for frequencies below 100 Hz.

All bearings have exhibited similar stiffness trend over the excitation frequency range under the various test conditions. There are few resonant spikes which distort the curves as shown in Figure 19, but the general evolution of the stiffness is linear especially in the horizontal direction and at low loads. The light and medium textured bearings have a tremendous effect on the horizontal stiffness. The average increase compared to the baseline bearing represents about 150% and 80% at static loads of 2,225 N and 5,340 N respectively (Figs. 19 and 20). The dimples contribute to stiffening the bearing horizontally by creating micro wedges at each oil pocket which act then in parallel and stiffen the bearing system. Increasing the dimple-density could have a reverse effect and reduces the stiffness at high loads (Fig. 20).

Surface-textured bearings also have a higher vertical stiffness but the relative increase is not as significant as in the horizontal direction. The average increase represents about 12% for TXT1 and is in the range of 20% for TXT2 and TXT4 regardless of the value of static load. This increase could be also attributed to the fact that the film thickness decreases when the number of dimples increases. TXT1 has almost no effect while TXT2 and TXT4 have the same K_{yy} increase.

As for the case of the baseline bearing, increasing the load shifts the stiffness to higher values.

The damping is only slightly affected by the surface texturing especially at the lowest load of 2,225 N (Fig. 21). Increasing the load reduces the overall damping for all bearing types (Fig. 22).

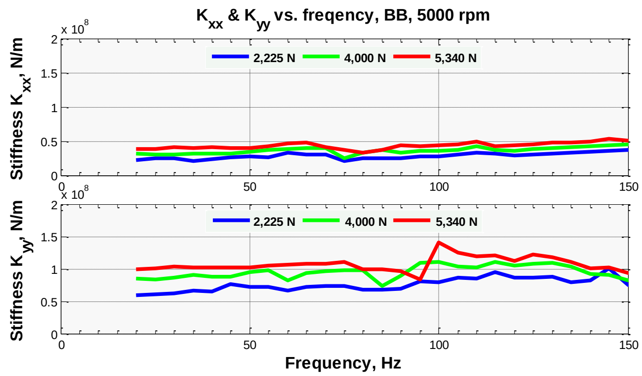

FIGURE 16. DIRECT STIFFNESS OF THE BASELINE BEARING AT 5,000 RPM AND VARIOUS LOADS

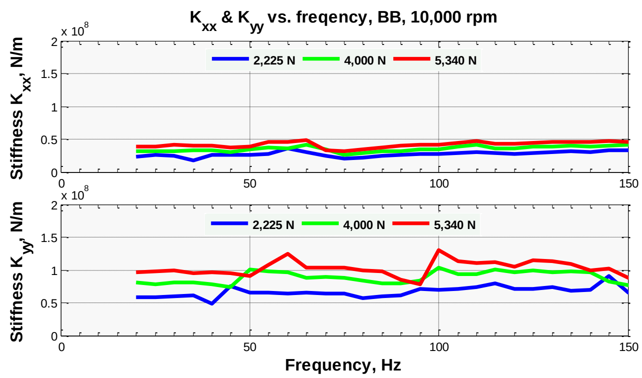

FIGURE 17. DIRECT STIFFNESS OF THE BASELINE BEARING AT 10,000 RPM AND VARIOUS LOADS

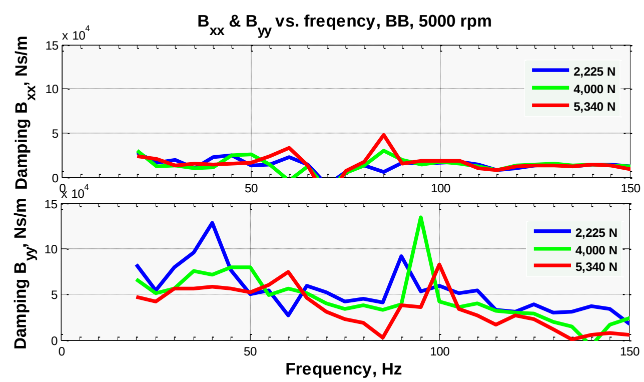

FIGURE 18. DIRECT DAMPING OF THE BASELINE BEARING AT 5,000 RPM AND VARIOUS LOADS

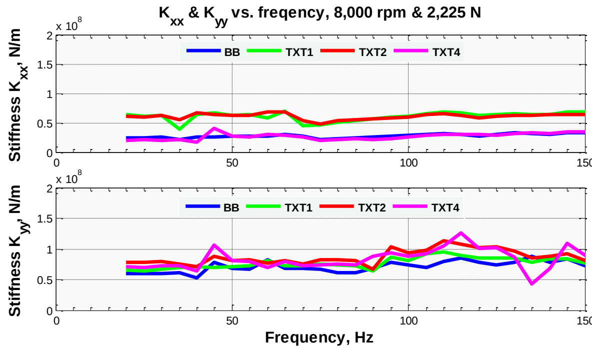

FIGURE 19. DIRECT STIFFNESS OF THE BASELINE AND TEXTURED BEARINGS AT 8,000 RPM AND 2,225 N

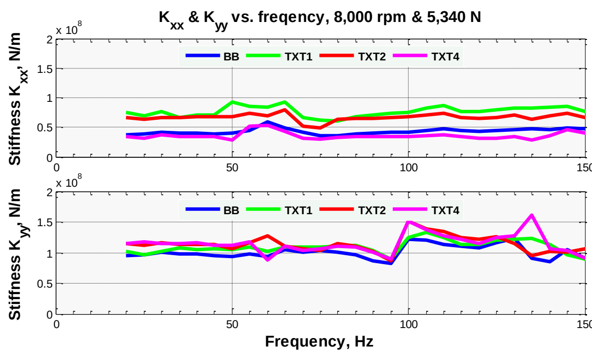

FIGURE 20. DIRECT STIFFNESS OF THE BASELINE AND TEXTURED BEARINGS AT 8,000 RPM AND 5,340 N

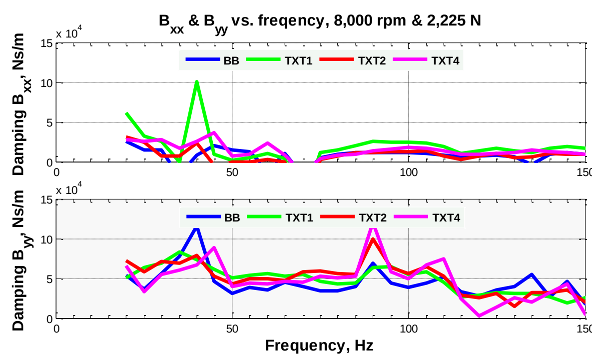

FIGURE 21. DIRECT DAMPING OF THE BASELINE AND TEXTURED BEARINGS AT 8,000 RPM AND 2,225 N

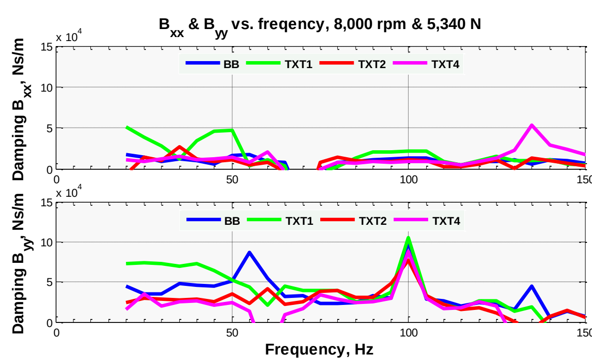

FIGURE 22. DIRECT DAMPING OF THE BASELINE AND TEXTURED BEARINGS AT A SPEED OF 8,000 RPM AND A LOAD OF 5,340 N

CONCLUSION & FUTURE WORK

In this experimental study, the effect of surface-texturing and dimple-density on the overall performance of plain journal bearings has been extensively investigated and analyzed. The main conclusions drawn from this work are listed below:

1- Lightly to medium textured bearing surfaces result in a better bearing stability and dense orbit.
2- Heavily textured-bearings run unstable and have lower load capacity and thinner oil film.
3- Textured journal bearings run hotter (about to 6 to 8 °) than plain smooth surface bearings.
4- Stiffness coefficients tend to slightly evolve in a linear fashion.
5- Radial load has a significant influence on bearing stiffness coefficients. The damping is slightly affected.
6- Lightly- and medium-textured bearings have tremendous influence on the direct horizontal stiffness coefficient representing up to 150% of that of the baseline bearing.
7- Medium- and highly textured bearings have a higher vertical direct stiffness.
8- Medium-textured surface bearing represents the optimum dimple-density as it leads to a stable bearing and increases both bearing direct stiffness coefficients.
9- All textured bearings have a slightly higher damping at low static loads.

Future work will consist on further analysis and characterization of dynamic properties including cross-coupled coefficients and stability maps of the studied bearings. The effect of clearance on the bearing performance as well as the influence of dimple-shape on the overall bearing steady-state and dynamic properties will also be investigated.

REFERENCES

[1] Etsion, I., 2005. “State of the art in laser surface texturing”. ASME J. Tribol., **127**(1), pp.248-253.

[2] Nilsson, B., Rosen, B. G., Thomas, T. R., Wiklund, D., and Xiao, L., 2004. “Oil pockets and surface topography: mechanism of friction reduction”. In Proceedings of the XI International Colloquium on Surfaces Chemnitz, Germany (Addendum).

[3] Etsion, I. and Sher, E., 2009. “Improving fuel efficiency with laser textured piston rings”. Tribol. Int., **42**(4), pp. 542-547.

[4] Costa, H. L. and Hutchings, I. M., 2007. “Hydrodynamic lubrication of textured steel surfaces under reciprocating sliding conditions”. Tribol. Int., **40**(8), pp. 1227-1238.

[5] Koszela, W., Pawlus, P., and Galda, L., 2007. “The effect of oil pockets size and distribution on wear in lubricated sliding”. Wear, **263**, pp. 1585-1592.

[6] Petterson, U. and Jacobson, S., 2004. “Friction and wear properties of micro textured DLC coated surfaces in boundary lubricated sliding”. Tribol. Lett., **17** (3), pp. 553-559.

[7] Lu, X. and Khonsari M. M., 2007, "An experimental investigation of dimple effect on the Stribeck curve of journal bearings". Tribol. Lett., **27**(2), pp. 169-176.
[8] Etsion, I., Halperin, G., and Becker, E., 2006. "The effect of various surface treatments on piston pin scuffing resistance". Wear, **261**, pp. 785-791.
[9] Brizmer, V., Kligerman, Y., and Etsion, I., 2003. "A laser surface textured parallel thrust bearing". STLE Tribol. T., **46**(3), pp. 397-403.
[10] Ryk, G. and Etsion, I., 2006. "Testing piston rings with partial laser surface texturing for friction reduction". Wear, **261**, pp. 792-796.
[11] Zhang, C. and Qiu, Z., 1998. "Effects of surface texture on hydrodynamic lubrication of dynamically loaded journal bearings". STLE Tribol. T., **41**(1), pp. 43-48.
[12] Yong, H. and Balendra, R., 2009. "CFD analysis on the lubrication behaviors of journal bearings with dimples". In Proc. 2009 IEEE, International Conference on Mechatronics and Automation, Changchun, China.
[13] Bouyer, J. and Fillon, M., 2010. "Experimental investigation on the influence of surface roughness and bearing materials on the friction coefficient during start-up". Proc. 2010 STLE Annual Meeting & Exhibition, Las Vegas, USA.
[14] Cupillard, S., Glavatskih, S., and Cervantes, M. J., 2008. "Computational fluid dynamics analysis of a journal bearing with surface texturing". Proc. IMechE, **222**, Part J, pp. 97-107.
[15] Wakuda, M., Yamauchi, Y., Kanzaki, S., and Yasuda Y., 2003. "Effect of surface texturing on friction reduction between ceramic and steel materials under lubricated sliding contact". Wear, **254**, pp. 356-363.
[16] Rahmani, R., Shirvani, A., and Shirvani H., 2007. "Optimization of partially textured parallel thrust bearings with square-shaped micro-dimples". STLE Tribol. T., **50**(3), pp. 401-406.
[17] Galda, L., Pawlus, P., and Sep, J., 2009. "Dimples shape and distribution effect on characteristics of Stribeck curve". Tribol. I., **42**(10), p. 1505-1512.
[18] Patent of Polish Republic, "Device for dynamic and static burnishing the flat and cylindrical surfaces". Patent n° 199622.
[19] Schroeder, M., 1970. "Synthesis of low-peak-factor signals and binary sequences with low autocorrelation". Information Theory, **16** (1), pp. 85–89.
[20] Rouvas, C., and Childs, D., 1993. "A parameter identification method for the rotordynamic coefficients of a high Reynolds number hydrostatic bearing". ASME J. Vib. Acoust., **115**(3), pp. 264–270.